

# Local Circuit Analysis with Integrated Large-Scale Recording of Neuronal Activity and Optogenetics

György Buzsáki

---

The Neuroscience Institute and Center for Neural Science  
New York University School of Medicine  
New York, New York





## Introduction

Numerous methods, such as macroscopic and microscopic imaging, molecular biological tools, and pharmacological manipulations, are available to study brain activity. However, all these indirect observations eventually should be converted back into a common currency—the format of neuronal spike trains—to understand the brain's control of behavior. Specific behaviors emerge from the interaction of neurons and neuronal pools. Studying these self-organized processes requires simultaneous monitoring of the activity of large numbers of individual neurons in multiple brain regions at the speed of neuronal communication in the behaving animal. Therefore, a major goal is to record from statistically representative samples of identified neurons from several local areas and to interact with them to probe their contribution to circuit function and behavior.

Local circuit analysis depends on three critical components: (1) neuron–electrode interface hardware for large-scale recording of neuronal activity, (2) effective spike-sorting methods, and (3) identification and targeted perturbation of specific neuronal types (Fig. 1). This chapter will present large-scale recording and analysis methods combined with focal optogenetic perturbations that can achieve these goals.

## Recording from Single and Multiple Single Neurons

Action potentials produce large transmembrane potentials in the vicinity of their somata. As a result, they can be sensed by placing a conductor (such as a saline-filled glass micropipette or the bare tip of an insulated wire) in proximity to a neuron (Fig. 2). Because neurons of the same class (e.g., pyramidal cells) generate identical action potentials, the only way to identify a given neuron from extracellularly recorded spikes is to move the electrode tip closer to its body ( $<20\ \mu\text{m}$  in cortex) than to any other neuron.

In general, there are three problems with this spike-amplitude-based approach using “sharp” electrodes. First, moving the electrode too close to the neuron affects its biophysical and firing properties. This is a particularly difficult problem in freely moving animals because even slight movement of the head may affect the discharge pattern. The second problem is related to the first: Because of electrode instability, long-term recordings from the same neurons are not practical with single “sharp” electrodes placed close to a single neuron. The third problem is the difficulty of simultaneously recording from large number of cells. For each neuron, a separate electrode is needed, resulting in excessive tissue damage. Because most anatomical wiring in the cortex is local, the majority of neuronal interactions, and thus computation, occurs in a small volume. In the cortex, this “small volume”

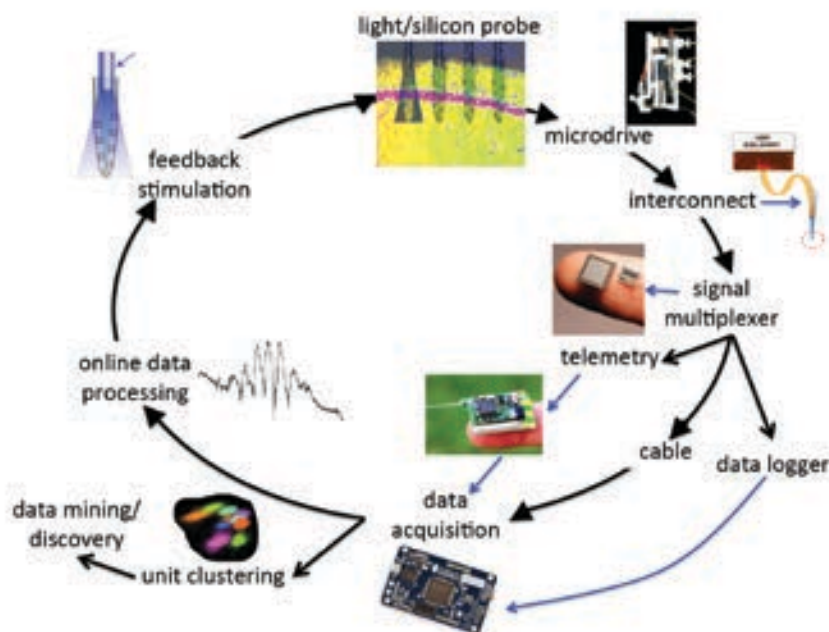


**Figure 1.** Flow chart showing components for large-scale recording of unit and LFP data, combined with optogenetic tagging of neurons and closed-loop perturbation of their activity for circuit analysis.

## NOTES

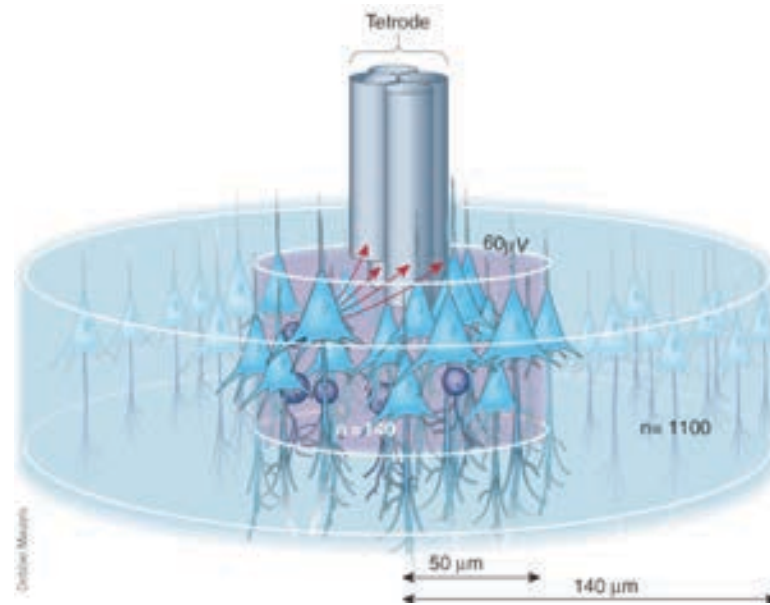


**Figure 2.** Unit isolation quality varies as a function of distance from the electrode. Multisite electrodes (e.g., wire tetrode) can estimate the position of the recorded neurons using triangulation. Distance of the visible electrode tips from a single pyramidal cell (triangles) is indicated by arrows. The spike amplitude of neurons ( $>60 \mu\text{V}$ ) within the gray cylinder ( $50 \mu\text{m}$  radius), containing  $\sim 100$  neurons, is large enough for separation using available clustering methods. Although the extracellularly recorded spike amplitude decreases rapidly with distance, neurons within a radius of  $140 \mu\text{m}$  (containing  $\sim 1000$  neurons in the rat cortex) can be detected. Improved recording and clustering methods are therefore expected to record from larger number of neurons in the future. Reprinted with permission from Buzsáki (2004), his Fig. 1.

corresponds to hypothetical cortical modules with mostly vertically organized layers of principal cells and numerous interneuron types. For example, in a cylinder of cortical tissue with a diameter corresponding to the extent of the dendritic tree of a pyramidal cell, hundreds to several thousand of other neurons cell bodies are located. Understanding such local computation requires improved methods that would allow for simultaneous recording of representative members of this closely spaced community but with minimal damage to neurons and wiring.

### Unit Isolation by Triangulation

Monitoring neurons from a distance has a major advantage: stability. A disadvantage is that with only one recording site, signals from many neurons that are the same distance from the tip provide the same magnitude signal, making single-cell isolation difficult. The use of two or more recording sites allows for the triangulation of distances because the amplitude of the recorded spike is a function of the distance between the neuron and the electrode (Fig. 2). Often, this task is accomplished with four spaced wires (dubbed “tetrodes”). Ideally, the tips are separated in three-dimensional space so that unequivocal triangulation is possible in a volume. Unfortunately, in practice the wires are cut flat, providing only two-dimensional (2D) monitoring of neurons, usually perpendicular to the main dipole generated by the action potential.

Cortical pyramidal cells generate extracellular currents that flow mostly parallel to their somadendritic axis. Nevertheless, tetrodes can “hear” hippocampal CA1 pyramidal cells as far as  $140 \mu\text{m}$  lateral to the cell body, although the extracellular spike amplitude decreases rapidly as a function of distance from the neuron. A cylinder with this radius contains  $\sim 1000$  neurons, which is the number of theoretically recordable cells by a single tetrode. Even so, in practice, only 5–15 neurons can be reliably separated using available algorithms. The remaining neurons may be damaged by the electrode, are silent, or are too small in amplitude, thus preventing reliable separation with only four monitoring sites. Nevertheless, wire tetrodes have numerous advantages over sharp-tip single electrodes, including a larger yield of units, low-impedance recording tips, and mechanical stability.

### Recording with Silicon Probes

An ideal recording electrode has a very small volume, so tissue injury is minimized. A wire electrode has only one useful part: the conductive tip; the rest consists of just ohmic conductor and inconvenient bulk. However, recording from large number of neurons with many tetrodes is possible only at the expense of extensive cell damage. The desire for large-scale monitoring of neurons from a small volume competes with the tissue damage inflicted by the electrodes.

Micro-Electro-Mechanical Systems (MEMS)–based recording devices can reduce the technical limitations inherent in wire electrodes because, by using the same amount of tissue displacement, the number of monitoring sites can be substantially increased. Whereas silicon probes keep the advantages of tetrode recording principles, they are substantially smaller. Further, multiple sites can be arranged over a longer distance, allowing for the simultaneous recording of neuronal activity in the various cortical layers. Six- to 8-shank probes with 8–32 sites on each probe can record from >100 well-separated neurons (Fig. 3). Because the geometrical distribution of the recording sites is known, the spatial relationship of the isolated single units can be determined. This latter feature is advantageous for studying the spatiotemporal representation and transformation of inputs by neuronal ensembles. Ideally, every part of a probe surface placed in the brain should have monitoring sites. However, this possibility is limited mainly by the width of the interconnect between the recording tips and the extracranial connector (although with the advent of signal multiplexers and on-chip active circuits, substantial volume and weight reduction can be achieved).

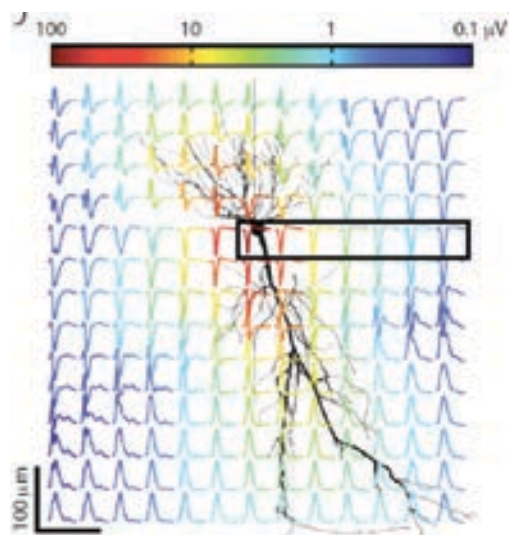


**Figure 3.** Extracellular contribution of an action potential (“spike”) to the LFP in the vicinity of the spiking hippocampal CA1 pyramidal cell. The peak-to-peak voltage range is indicated by the color of the traces. Note that the spike amplitude decreases rapidly with distance from the soma, without a change in polarity within the pyramidal layer (approximately the boxed area), in contrast to the quadrupole (i.e., reversed polarity signals both above and below the pyramidal layers) formed in the somatodendritic axis. Reprinted with permission from Buzsáki et al. (2012), their Fig. 2*d*.

A further advantage of silicon probes is their ability to sample the extracellular current effectively (Fig. 4). A requirement for understanding the transformation of inputs by a neuron or neuronal assemblies is information about both their input and output. Unfortunately, no simple method is available for monitoring all inputs at the resolution of dendrites and spines of single neurons in behaving animals. However, membrane currents generated by neurons pass through the extracellular space. These currents then can be measured by electrodes placed outside the neurons. The local field potential (LFP, or more correctly, the mean local voltage) recorded at any given site reflects the linear sum of numerous overlapping fields generated by current sources (current from the intracellular space to the extracellular space) and sinks (current from the extracellular space to the intracellular space) distributed along multiple cells. LFP measurements, combined with recording of neuronal discharges, are an efficient tool for studying the influence of cytoarchitectural properties (e.g., cortical lamination, distribution, size, network connectivity) of neural elements on electrogenesis. However, a large number of observation points, combined with decreased distance between the recording sites, is required to achieve high spatial resolution and for interpreting the underlying cellular events. Recording the voltage gradients by geometrically arranged sites of silicon probes allows current densities to be calculated in order to estimate the mean input to the neuron group in the recorded volume.

### Isolation and Identification of Neurons by Extracellular Signatures

An indispensable step in spike-train analysis is the isolation of single neurons on the basis of extracellular features. Spike-sorting methods fall into two broad classes. The first class attempts to separate spikes on the basis of amplitude and waveform variation; the second, triangulation method separates units on the basis of their spatial location. Unfortunately, neither method is satisfactory. When neurons are strongly activated, their amplitude, rise time, decay time, and spike width change as a function of both the membrane potential before the spike and the immediate firing history of the neurons. The spike amplitude variation is most substantial during complex spike-burst production, with as much as 80% amplitude reduction, primarily because of  $\text{Na}^+$  channel inactivation. Therefore, amplitude and waveform-based classification programs will separate action potentials from a single neuron as if they were emitted by many. The amplitude and waveform variability of the extracellularly recorded spike is the major cause of unit isolation errors.



## NOTES

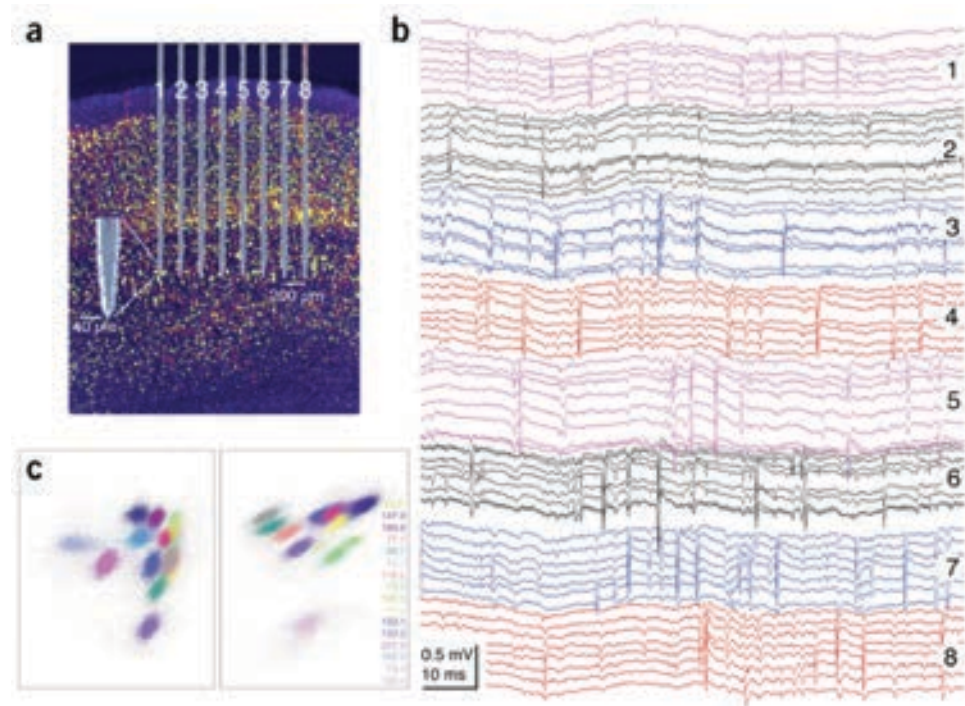


**Figure 4.** High-density recording of unit activity in the somatosensory cortex of the rat. **a**, Placement of an 8-shank silicon probe in layer 5. The 8 recording sites at the edges of the tip (inset) are connected to the extracranial electronics via 2  $\mu\text{m}$  interconnects. Scale bars, 200  $\mu\text{m}$  and 40  $\mu\text{m}$ . **b**, A short epoch of raw recording, illustrating both field and unit activity (1 Hz–5 kHz). Note the presence of spikes on several sites of the same shank (color-coded) and the lack of spikes across the different shanks, indicating that electrodes placed  $\geq 200$   $\mu\text{m}$  laterally record from different cell populations. **c**, 2D views of unit clusters (out of 28 possible views from an 8-site probe) from one shank. Clusters are color-coded. Numbers on right in **c** represent “isolation distance”; i.e., larger numbers indicate better neuron isolation. Reprinted with permission from Buzsáki (2004), his Fig. 2.

The second, triangulation approach is based on the tacit assumption that the extracellularly recorded spikes emanate from point sources. However, every part of the neuronal membrane is capable of generating action potentials, and what is observed in the extracellular space results from the complex geometry of neuron and spike propagation within the neuron. The extent of the somadendritic back-propagation of the action potential varies as a function of the excitatory and inhibitory inputs impinging on the neuron, as well as the state of various other conductances. The spike recorded in the extracellular space sums up the integrated signals from both soma and large proximal dendrites. Thus, the extent of somadendritic spike back-propagation can affect the estimation of the neuron’s virtual “point source” location and may place the same neuron at different locations, resulting in omission errors of unit isolation.

A further problem with the point-source assumption for action potentials is that the somatic origin is not always resolvable with distant recording sites. For example, in the rat neocortex, extracellular spikes can be recorded from the apical shaft of layer 5 pyramidal neurons as far as 500  $\mu\text{m}$  from the cell body. As a consequence, electrodes placed in layer 4, for example, can equally

record from layer 4 cell bodies or apical dendrites of deeper neurons. Large neurons in the primate cortex are especially prone to such misclassification errors because their spikes can be recorded from several hundred micrometers from the cell bodies.

To a large extent, these sources of unit separation errors can be reduced by recording at multiple sites parallel with the axodendritic axis of the neurons. However, most triangulation methods visually analyze 2D projected datasets simultaneously. With multiple site-recorded data, successive comparisons of the various possible projections generate cumulative errors of human judgment. As a result, a major motivation behind the development of efficient automatic clustering methods of high-dimensional data is to eliminate cumulative human errors.

The geometrically defined recording sites of silicon probes have additional advantages because, in addition to the output spikes, they can record the mesoscopic LFP signal that reflects the cooperative nature of input and synchronous activity of nearby neurons. With high enough density of recording sites, the afferents to the neurons can be precisely identified in architecturally regular structures (Fig. 5).

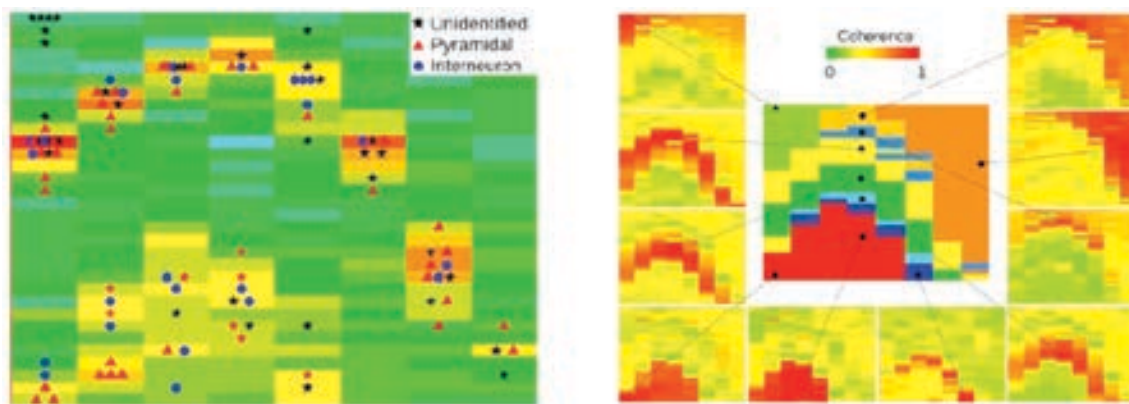


**Figure 5.** Generation of extracellular field potentials. Left, Distribution of high-frequency power ( $300 \pm 10$  Hz) outlines the cell body layers of the hippocampus. The  $32 \times 8$  color matrix represents the power values on the 256 sites of the silicon probe. Each rectangle represents a  $300 \mu\text{m}$  (intershank distance)  $\times$   $50 \mu\text{m}$  (vertical intersite distance) area to mimic the 2D geometry of the probe coverage of the CA1 and dentate areas. Clustered neurons, assigned to the largest amplitude recording sites, are superimposed on the power map. Right, outer squares: Coherence maps of gamma activity (30–90 Hz). The 10 example sites (black dots) served as reference sites, and coherence was calculated between the reference site and the remaining 255 sites. Note how gamma coherence effectively outlines dendritic layers. Middle, composite figure of the combined coherence and power maps. Recordings were made from a freely behaving rat during foraging. Reprinted with permission from Berényi et al. (2014), their Fig. 5.

## Local Circuit Analysis Using Combined Silicon Probe Recordings and Optogenetics

After isolating single neurons, the units should be classified into known cell groups of the cortex. This is a very important requirement because cortical networks consist of several neuronal classes, each having a specific computation task. Such classification will greatly improve the interpretation of hard-earned physiological data. The recent advent of optogenetics offers a solution for identifying specific, genetically defined neuronal subtypes in blind extracellular recordings by expressing light-sensitive opsins in a given neuronal population. Both activation and silencing strategies can be used for this purpose while implementing transgenic or virus infection methods. One important task for local circuit analysis is the simultaneous monitoring of all light-responsive neurons near the recording electrodes and estimating the fraction of the optogenetically responsive neurons (Royer et al., 2012; Stark et al., 2012). Integrated recording–optogenetic methods can be used to accomplish at least three goals:

- (1) Identifying genetically labeled neurons (optical “tagging”),
- (2) Characterizing and classifying neuron types physiologically, and
- (3) Testing the causal roles of the identified neurons on the performance of local circuits.

Because neurons are both embedded in circuits and contribute to circuit function, perturbing them can bring about secondary changes that need to be separated from the primary action of optical stimulation. A major problem with most available methods for identifying neurons and analyzing local circuits arises from the use of large-diameter optical fibers for brain surface illumination at high light power. Such technical problems can be significantly reduced by etching small-core ( $\leq 50 \mu\text{m}$ ) optical fibers to a point ( $\leq 10 \mu\text{m}$ ) and mounting them close ( $< 40$ – $50 \mu\text{m}$ ) to the recording sites (Fig. 6). Hybrid devices that combine silicon probes with etched optical fibers allow the use of extremely low-power stimulation, eliminate photoelectric artifacts, and reduce artificially induced overlapping spikes. Experiments have shown that  $< 5 \mu\text{W}$  of light ( $\leq 0.1 \text{ mW/mm}^2$ ) is sufficient to activate ChR2-expressing neurons *in vivo*. Synchronous spiking can be minimized by using sinusoid or Gaussian waveform stimulation, as opposed to pulses. That is because neurons that express different amounts of opsins and experience different intensities at varying distances from the light source are expected to have variable thresholds for spike generation and, therefore, respond at shifting phases of the light stimulus.

The low light-intensity requirement can eliminate the need for benchtop lasers and optical cables that restrain the freedom of the animal’s movement. Instead, miniature light emitting diodes (LEDs) and/or laser diodes can be coupled to short, small-diameter ( $50 \mu\text{m}$ ) multimode fibers and attached directly to the shanks of

## NOTES

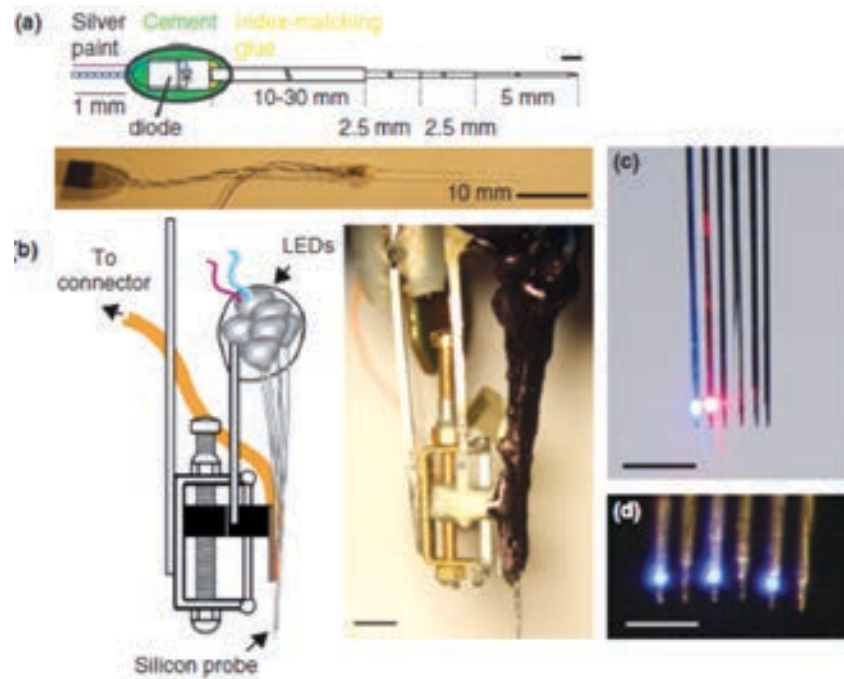


**Figure 6.** Diode probes for optogenetically identifying interneurons. *a*, Schematic of a single LED-fiber assembly. The LED is coupled to a 50 mm multimode fiber, etched to a point at the distal (brain) end. Scale bar, 10 mm. *b*, Left, Schematic of a drive equipped with a 6-shank diode probe with LED-fibers mounted on each shank. Etched optical fibers are attached ~40 mm above the recordings sites on the silicon probe shanks. Right, Picture of the drive depicted on the left. Scale bar, 3 mm. *c* and *d*, Local delivery of light. Magnified frontal view of the 6-shank diode probe equipped with diode-coupled optical fibers. *c*, Two adjacent shanks are illuminated with blue and red light. Scale bar, 1 mm. *d*, 3 shanks are illuminated with blue light. Scale bar, 0.5 mm. Reprinted with permission from Roux et al. (2014), their Fig. 1.

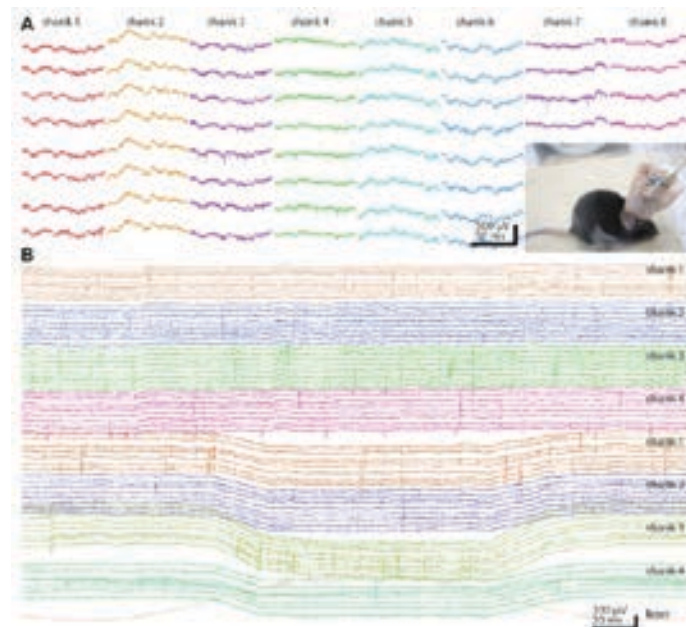


**Figure 7.** Unit and LFP recordings from the mouse. *A*, Chronic recordings from a mouse using an 8-shank 64-site silicon probe (diode probe). 100 ms epochs from each shank are shown. Inset: head stage with silicon probe, microdrive, and 64-channel signal multiplexer, surrounded by copper mesh shielding. The freely moving mouse is connected to the equipment by an ultra-flexible cable. *B*, Two 4-shank, 32-site probes were placed in the nucleus accumbens (top shanks 1–4) and ventral tegmental area (VTA; bottom shanks 1–4) in a TH-Cre;Ai32 mouse, expressing ChR2 in tyrosine hydroxylase-expressing neurons. One of the shanks in the VTA also contained an optical fiber for light delivery. Note VTA neuronal responses to 472 nm (bottom red trace) laser light stimulation. Reprinted with permission from Berenyi et al. (2014), their Fig. 13.



a silicon probe or tetrode (Fig. 6). The small size and light weight of these integrated “diode probes” (1.0–2.5 g) enable fast, multisite, and multicolor optogenetic manipulations in freely moving animals with concurrent monitoring of the manipulated neurons (Fig. 7).

In addition to optogenetics, numerous classification schemes based on a variety of physiological criteria have been developed to assign extracellular spikes to putative interneurons and pyramidal cells and their putative subtypes. These include waveform

features, firing rate statistics in different brain states, embeddedness in various population activities, firing patterns characterized by their autocorrelograms, and putative monosynaptic connections to other neurons. However, the “ground truth” of these classifying methods is essentially missing. An important goal of the optogenetic approach is to assist in the identification of distinct subtypes of neurons within individual, molecularly identified classes. However, in a single experiment, optogenetic methods can assist in the identification of only one or

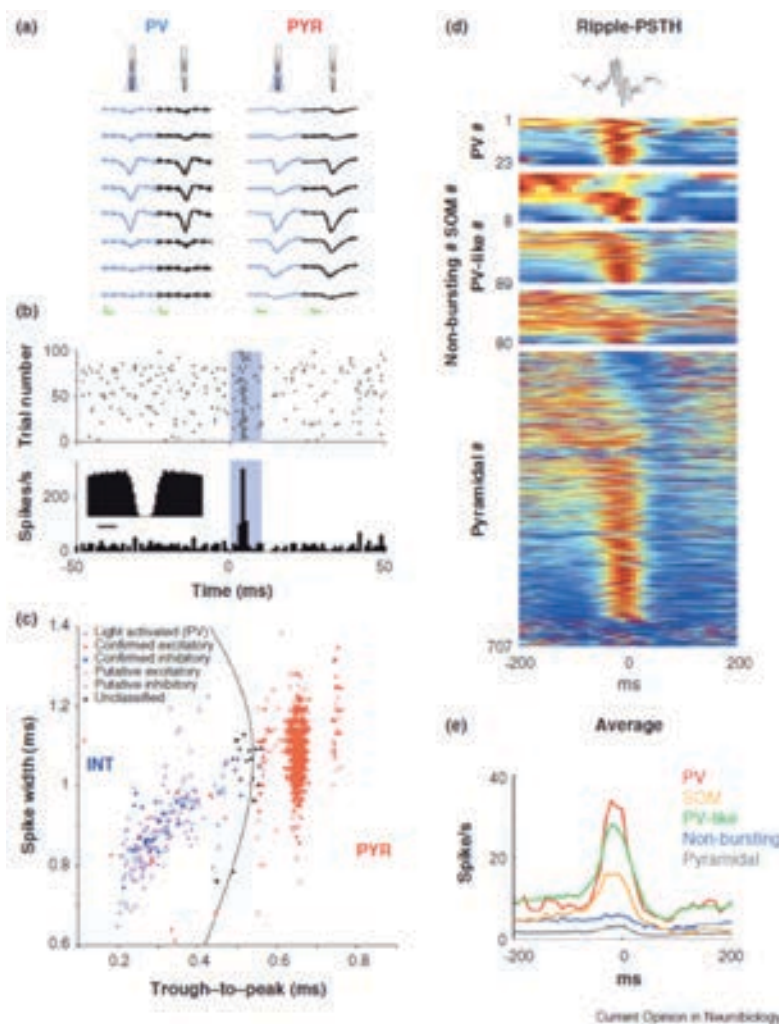


**Figure 8.** Optogenetic identification of interneurons. *a*, Right, Unfiltered spontaneous (black) and light-induced (blue) waveforms of a parvalbumin-expressing interneuron (PV) and a pyramidal cell (PYR) at 8 recording sites. Note the similarity of the waveforms with and without illumination. Mean and SD; calibration, 0.25 ms, 50  $\mu$ V. *b*, Diode-probe-induced unit firing in the hippocampal CA1 region (blue shaded area superimposed on the raster plot [top] and the histogram [bottom]; 4 mW at fiber tip). Inset: Autocorrelogram shows a shape typical for fast-spiking PV interneurons. *c*, Clustered units are tagged as excitatory or inhibitory on the basis of monosynaptic peaks/troughs in cross-correlation histograms (filled blue and red symbols) and/or response to locally delivered 50–70 ms light pulses (filled violet symbols) in transgenic mice expressing ChR2 in PV cells. Untagged units (empty symbols) are classified as putative excitatory pyramidal cells (PYRs) or inhibitory interneurons (INTs) according to waveform morphology; untagged units with low classification confidence are also shown in black (“unclassified”). *d*, Optogenetic identification of interneuron classes, including here PV-expressing and somatostatin (SOM)-expressing interneurons, allows studying their relationships to network patterns such as sharp-wave ripple events. Top, Single ripple. Each row represents the color-coded peri-ripple histogram of the firing rate computed for individual neurons. PSTH, peristimulus time histogram. *e*, Average firing rate observed for the different cell categories (PV, SOM, PV-like, nonbursting, and pyramidal). Reprinted with permission from Royer et al. (2012), their Supplementary Figs. 5a–d.

## NOTES

two neuron types. To be able to identify more diverse components of circuits, an iterative refinement of a library of physiological parameters is needed so that, subsequently, the various neurons can be recognized reliably by using purely physiological criteria without the need for optogenetics (Fig. 8).

Dramatic reduction in light intensity, combined with dense recording of the surrounding neurons, allows one to perform single-neuron stimulation and to estimate the absolute numbers of directly driven neurons in a small illuminated volume. Being able to assess the fraction of neurons that can affect a particular physiological pattern, perception, memory, or overt behavior is an important goal of circuit analysis.

## References

*Extensive and excellent technical reviews, written by various experts in the field, are available for further reading, most of which are listed below.*

- Berényi A, Somogyvári Z, Nagy AJ, Roux L, Long JD, Fujisawa S, Stark E, Leonardo A, Harris TD, Buzsáki G (2014) Large-scale, high-density (up to 512 channels) recording of local circuits in behaving animals. *J Neurophysiol* 111:1132–1149.
- Buzsáki G (2004) Large-scale recording of neuronal ensembles. *Nat Neurosci* 7:446–451.
- Buzsáki G, Anastassiou CA, Koch C (2012) The origin of extracellular fields and currents—EEG, ECoG, LFP and spikes. *Nat Rev Neurosci* 13:407–420.
- Gold C, Henze DA, Koch C, Buzsáki G (2006) On the origin of the extracellular action potential waveform: a modeling study. *J Neurophysiol* 95:3113–3128.
- Harris KD, Henze DA, Csicsvari J, Hirase H, Buzsáki G (2000) Accuracy of tetrode spike separation as determined by simultaneous intracellular and extracellular measurements. *J Neurophysiol* 84:401–414.
- Hazan L, Zugaro M, Buzsáki G (2006) Klusters, NeuroScope, NDManager: a free software suite for neurophysiological data processing and visualization. *J Neurosci Methods* 155:207–216.
- Henze DA, Borhegyi Z, Csicsvari J, Mamiya A, Harris KD, Buzsáki G (2000) Intracellular features predicted by extracellular recordings in the hippocampus *in vivo*. *J Neurophysiol* 84:390–400.
- Roux L, Stark E, Sjulson L, Buzsáki G (2014) *In vivo* optogenetic identification and manipulation of GABAergic interneuron subtypes. *Curr Opin Neurobiol* 26C:88–95.
- Royer S, Zemelman BV, Losonczy A, Kim J, Chance F, Magee JC, Buzsáki G (2012) Control of timing, rate and bursts of hippocampal place cells by dendritic and somatic inhibition. *Nat Neurosci* 15:769–775.
- Stark E, Koos T, Buzsáki G (2012) Diode probes for spatiotemporal optical control of multiple neurons in freely moving animals. *J Neurophysiol* 108:349–363.